

Research Article

Computer-Aided Diagnosis of Acute Lymphoblastic Leukemia Using a Novel CAE-CNN Framework

Mohammed Mansoor AL-Hammadi 
Institute of Applied Arts
Middle Technical University
Baghdad,
Iraq
mohamed_mansour@mtu.edu.iq

ARTICLE INFO

Article History

Received: 31/05/2024

Accepted: 06/07/2024

Published: 31/12/2024

This is an open-access article under the CC BY 4.0 license:

<http://creativecommons.org/licenses/by/4.0/>**ABSTRACT**

Acute lymphoblastic leukemia (ALL) is a main health problem throughout the world. Therefore, fast and exact diagnosis is the most crucial factor for providing efficient management and treatment methods. The conventional diagnostic tools, based on the morphological and cytochemical investigation of blood and bone smears, are usually not specific and laborious. Thus, they often result in diagnostic errors and delay in treatment initiation. In this paper, ALL-diagnosing methods based on the convolutional autoencoder (CAE) was proposed to reduce the amount of data, and then convolutional neural network (CNN) was applied to identify ALL. The design method employed deep neural networks to recognize the features of the cells in question and then distinguish them as either leukemic or healthy cell types. The proposed laboratory method, with the use of the curated datasets of annotated pathological images of normal lymphoid progenitor cells, aimed to tackle the challenges related to the lack of curated datasets with annotated images of these cells. These challenges are believed to be linked to imprecise and time-consuming leukemia diagnosis and cure process. The simulated results confirmed the efficiency of the suggested technique, where CAE showed a correlation coefficient of 0.987 for lymphoblastic cells

Keywords: *Acute lymphoblastic leukemia, Convolutional Autoencoder, Convolutional Neural*

1. INTRODUCTION

Acute lymphoblastic leukemia (ALL) is an overwhelming health challenge in modern oncology. The Global Cancer Observatory showed that about 1 million people were diagnosed with leukemia that year, with 627,105 death, highlighting the pressing need for well-developed diagnostic and therapeutic procedures [1]. Even though ALL majorly affects the pediatric patient population, the adult patient population still considerably contributes to its complexity and gravity, making its management strategies very complex. The difference in the capacities of cancer management infrastructure between high-income and low-to-middle-income countries emphasizes the relevance of visionary and swift diagnosis tools to combat the rising morbidity rates related to ALL.

For patients with ALL, the precise diagnosis of malignant blasts is particularly different from that of normal lymphatic lineage, thus producing diagnostic errors and ambiguities. Routine examination is conducted in terms of morphological, cytochemical, and immunophenotypic criteria, of which clinicians are usually short of experience with or without subjective interpretation, leading to necessary invasive procedures. In addition, the diagnostic dilemma is overwhelmed by limited datasets that are inadequate to cover everything about normal lymphoid precursors, thereby reducing the complexity of creating computer-aided diagnosis (CAD) appropriate for untargeted leukemia detection. As explained earlier, the current diagnostic approaches suffer from some deficiencies. Therefore, innovative diagnostic techniques that could benefit from the recent advances in computational techniques and deep learning algorithms with very high accuracy must be considered and adopted in response to these pressing needs. Many approaches have been proposed at present.

2. RELATED WORKS

In this section, some related works were reviewed to further understand ALL diagnosis and its.

The utilization of neuro-fuzzy and group data handling methods was investigated in [2] for diagnosing childhood acute leukemia through complete blood count tests, incorporating principal component analysis (PCA) to enhance diagnostic accuracy. Patient/non-patient differentiation was efficiently achieved via the adaptive neuro-fuzzy inference system, and distinguishing between specific disease types may necessitate additional pre-processing operations such as feature reduction. In [3], patients diagnosed with chronic myeloid leukemia (CML) were identified using the BCR-ABL1 diagnostic test and six consecutive prior years of blood cell counts in the largest U.S. integrated healthcare system. Machine learning (ML) models (XGBoost and least absolute shrinkage and selection operator [LASSO]) that were trained on blood cell counts at different time intervals before diagnosis demonstrated improved predictive ability. An ALL detection technique was introduced in [4], where three models incorporating fully connected and/or dropout layers in the ResNet50 architecture were presented. The model with optimal training performance was chosen for feature extraction. Logistic regression, support vector machine (SVM), and random forest (RF) were employed for ALL classification, and their performances were compared. A study [5] explored the application of transcriptomic-based ML to predict acute myeloid leukemia (AML) status across 12,029 samples from 105 studies. Employing data-driven and high-dimensional approaches, the study suggested the potential for a near-automated workflow in AML diagnosis through a scalable combination of transcriptomics and ML, providing risk prediction, differential diagnosis, and subclassification capabilities. An ML analysis of pediatric ALL [6] showed the significance of clinical, phenotypic, and environmental variables in identifying the underlying causes of the disease. The study included 50 pediatric patients and utilized four supervised ML algorithms (classification and regression tree [CART], RF, gradient boosted machine, and C5.0 decision tree). Another study [7] introduced an ML model (RF) for efficient diagnosis of AML by detecting and classifying immature leukocytes. Utilizing images from The Cancer Imaging Archive, image format conversion, multi-Otsu thresholding, and morphological operations were employed for segmentation, extracting 16 features, including two novel nucleus color features. Study [8] aimed to develop diagnostic systems for early leukemia detection by using ALL image databases (ALL_IDB1 and ALL_IDB2). Three systems were proposed as follows: 1) artificial neural network (ANN), FFNN, and SVM based on hybrid features; 2) convolutional neural network (CNN) models (AlexNet, GoogleNet, and ResNet-18) with transfer learning for early leukemia detection; and 3) hybrid CNN-SVM technologies. In [9], an integrative analysis of RNA-seq data from BCR-ABL1-positive acute leukemia samples identified p190 BCR-ABL1, a novel MAP2K2 gene fusion, and clinically significant mutations. Scoring algorithms and ML demonstrated high diagnostic performance not only for the original 12 BCR-ABL1-positive cases but also for 427 public gene expression datasets from acute leukemia, irrespective of specific genetic aberrations. Study [10] employed artificial intelligence (AI)/ ML predictive modeling on morphological and immature fraction-related parameters derived from complete blood count (CBC) to differentiate various types of leukemias at the pre-microscopic level. By utilizing routine and research CBC parameters from 1577 subjects with hematological neoplasms, the study demonstrated the predictive capacity of research CBC items through statistical analysis, heatmaps, and PCA. Study [11] proposed an automated leukemia detection process using ML and image processing techniques on a dataset comprising blood smear images from patients with and without leukemia. Image segmentation employed K-means clustering, marker-controlled watershed segmentation, and HSV color-based segmentation, extracting distinctive features from segmented lymphocyte images. The SVM classifier was then employed for leukemia classification into AML, ALL, CML, or CLL. In [12], an ML model was trained on a multicentric dataset of 2177 individuals from 27 organizations, 25 cities, 15 countries, and four continents, utilizing 26 probe sets and age features to classify AML or healthy status. Study [13] proposed modifications to CNN topologies for precise recognition of nonmalignant and malignant cells, particularly focusing on automatic leukemia detection using CAD models. In a single-center study, a deep learning model was developed for classifying leukemic B-lymphoblasts, achieving a test accuracy of 95.59% through data augmentation methods and transfer learning techniques to enhance performance on a limited dataset. A model was developed in [14] to classify acute leukemias, including acute promyelocytic leukemia, and differentiate them from non-neoplastic cytopenia by using data from 531 patients. The model involved unsupervised learning with Gaussian mixture model and Fisher kernel methods on flow cytometry (FC) data, followed by supervised SVM classification. Study [15] introduced a novel method utilizing ML algorithms on leukemia GSE9476 cell microarrays to predict the initial leukemia disease. By employing decision trees, naive Bayes (NB), RF, gradient boosting machine, linear regression, SVM, and a novel approach combining logistic regression with decision tree parameters, the proposed ensemble LDSVM model achieved an impressive accuracy of up to 99%. Study [16] focused on ML-based treatment outcome classification for patients with ALL under 18 years of age and analyzed data from 241 pediatric patients treated at MAHAK Hospital in Iran from 2012 to 2018. The dataset included demographic, medical, and treatment-related complication features. By employing common classification algorithms, the XGBoost algorithm achieved an accuracy of 88.5% in the first scenario, whereas SVM emerged as the superior model in the second scenario, with an accuracy of 94.90%. Study [17] focused on employing optimal ML algorithms to detect leukemia in its early stages. Peripheral blood smear (PBS) images, which are microscopic representations of blood samples, were collected, preprocessed, and segmented based on pixels. The enlarged

portions of the affected areas were utilized for feature extraction, and CNN was employed for classification, achieving accurate leukemia detection. Study [18] systematically evaluated existing ML-based algorithms for leukemia detection and classification using PBS images. The ML techniques achieved an accuracy rate exceeding 93.5% in the PBS image analysis for leukemia detection, showcasing the potential of ML applications in exceptional leukemia diagnosis from PBS images. In another study [19], leukemia cancer data with 7129 genes and 72 patients (47 patients with cancer and 25 controls), were obtained from the Kent Ridge Biomedical Data Repository, USA. Five feature selection techniques, including t-test, Wilcoxon sign rank sum test, RF, Boruta, and LASSO were used. Six classifiers, namely Adaboost (AB), CART, ANN, RF, linear discriminant analysis (LDA), and NB, were employed. Study [20] introduced two automated classification models by using blood microscopic images for leukemia detection. Transfer learning, which employs a pre-trained deep CNN (AlexNet), was utilized. The first model involved pre-processing, feature extraction, and classification with various classifiers, and the second model fine-tunes AlexNet for feature extraction and classification. Experiments were conducted on a dataset of 2820 images. Various ML algorithms were employed in [21] to create an automated analysis for classifying normal and chronic lymphocytic leukemia cases in clinical FC. Among them, the gradient boosting algorithm demonstrated the best results, with the XGBoost classifier. An Internet of Medical Things framework was proposed in [22] for efficient leukemia identification, utilizing cloud computing to connect clinical devices and facilitate real-time coordination for testing, diagnosis, and treatment. The framework employed dense CNN (DenseNet-121) and residual CNN (ResNet-34) for leukemia subtype identification, utilizing publicly available datasets ALL-IDB and ASH image bank. An algorithm was proposed in [23] for early-stage leukemia detection using image processing and ML classification techniques. K-means clustering segment images and linear SVM were applied to classify cancerous and non-cancerous cells. The algorithm, which was validated on the ALL-IDB dataset with 368 images, achieved 95% accuracy and approximately 93% precision. Two classification models were proposed in [24] for ALL detection, utilizing the ALL-IDB2 dataset of blood microscopic images. The hybrid model involved image pre-processing, feature extraction with AlexNet, and classification using SVM, kNN, XGBoost, and decision trees. The AlexNet-based model employed image pre-processing and conducts feature extraction and classification using AlexNet. A novel deep learning algorithm was proposed in [25] for leukemia diagnosis through microscopic blood sample images. The architecture incorporated squeeze and excitation learning to enhance feature representation, emphasizing channel associations. The model exhibited improved diagnostic performance on leukemia datasets (ALL_IDB1 and ALL_IDB2) through extensive experiments on cropped and full-size images, addressing data scarcity and enhancing overall accuracy.

While giving encouraging hints to the overall progress in the field of medical imaging and diagnostic technologies, the exact diagnosis of ALL still seems to be unclear. The main diagnostic procedures, which crucially rely on morphologic and cytochemical examination of blood and bone marrow samples, are often very labor-intensive and time-consuming and the results are relatively subjective. Further, the digital methods' diagnostic accuracy can be diminished by the subjectivity and variability between the observers, as well as by the fact that it relies on subjective criteria only, which can result in misdiagnoses and treatment delays.

This work indexes the current body of research by establishing a new method for ALL diagnosis, with a synthesis of CAE for feature extraction and CNN for classification. The proposed method centers on the use of powerful deep learning models to extract complex features from lymphoblast cell photos, followed by accurate classification as leukemia or non-cancer cells.

The methodology comprises the training of CAE to obtain the key cell morphological features of the lymphoblast images and then transforming these features into the inputs of CNN, which is parametrized for classification. The proposed approach let solving the feature extraction and classification tasks together in the same framework. Thus, improvements in diagnosis accuracy and efficiency are possible, which could lead to early diagnosis and timely intervention.

3. DATASET

The dataset used in this study was thoroughly prepared in the Laboratory Oncology Unit of Dr. B.R.A ICTR and Human Genetics Institute, All India Institute of Medical Sciences (AIIMS), New Delhi, India. The slides were conscientiously made by the experimental method using marrow aspirate from both control- and patient subjects and contained normal cells obtained from all uninvolved individuals and cancer cells acquired from patients newly diagnosed with B-cell ALL (B-ALL). The preparation process involved placing the slides on a Jenner-Giemsa stain to help highlight the desired cells. Then, the slides were observed under a Nikon microscope with a Nikon DS5M camera for capturing 2560 × 1920 size images of the slide. The format for saving the images was BMP.

The slide images that were recorded using a microscope were picked up after word-by-word debugging by an onco-pathologist, who is a specialist in that field, to identify cells of interest, particularly lymphoblasts, which

are the leading cause of B-ALL. As the examination of the image produced a considerable number of cell types, including lymphoblasts, plasma cells, and red blood cells, the lymphoblasts must be separated and marked out for further study. The lymphoblast identifier was created by a single pathologist specializing in oncology, who was aware of the significance and accuracy of maintaining consistency.

For 2 years, the dataset compilation process encountered variability in stain color among subjects' slides. A stain color normalization technique known as the GCTI-SN method was employed to mitigate this variability, utilizing a reference image to standardize stain colors across images. Subsequently, cell images were segmented from the microscopic images by using an in-house segmentation pipeline, which successfully separated cells even within clustered formations. This meticulous workflow culminated in the creation of a dataset comprising 7108 single-cell images obtained from 118 subjects, including 49 control (healthy) subjects and 69 cancer subjects.

Given the inherent variations in cell image sizes, a standard size of 350×350 was uniformly achieved for each image by padding columns and rows with zero intensity, ensuring consistency across the dataset [26].

4. BASIC CONCEPTS

In this section, the basic concepts and networks needed for introducing the proposed method were explained,

4.1 CNN

CNN is a type of feedforward neural network designed for automatic feature extraction through convolutional structures. In contrast to traditional methods requiring manual feature extraction, CNNs automatically learn and extract features. The architecture is inspired by visual perception, where artificial neurons correspond to biological neurons, CNN kernels act as receptors for various features, and activation functions mimic the transmission of neural signals above a threshold.

CNNs offer several advantages compared with general ANNs. First, they employ local connections, where each neuron connects to only a small number of neurons in the previous layer, reducing parameters and accelerating convergence. Second, weight sharing allows a group of connections to share the same weights, further reducing parameters. Third, down-sampling through pooling layers leverages local image correlations, reducing data size while preserving essential information and eliminating trivial features. These three characteristics establish CNNs as a prominent algorithm in the deep learning field [27]. This network consists of different layers as follows:

- Convolutional Layer:

The convolutional layer is the fundamental building block of a CNN. It performs convolution operations on the input data by using filters or kernels. These filters slide over the input to detect spatial patterns such as edges, textures, and shapes. This process involves sliding a window over the image, learning features through shared weights and biases, and creating feature maps that capture local receptive fields. Equations 1 and 2 describe the output matrix size without padding and the convolution operation, and Equation 3 illustrates the output size with padding to maintain the input image size as follows:

$$NXN * fXf = N - F + 1, \quad [1]$$

$$O = \sigma(b + \sum_{i=0}^{31} \sum_{j=0}^{31} w_{i,j} h_{a+i,b+j}), \quad [2]$$

$$NXN * f * f = \frac{(N+2P-f)}{(S+1)}, \quad [3]$$

where O represents the output, P denotes padding, s refers to stride, b means bias, σ is the sigmoidal activation function, w is a 32×32 weight matrix of shared weights, and $h_{x,y}$ is the input activation at position x, y. Convolutional layers help the network automatically learn hierarchical features from the input [28].

- Batch Normalization:

Batch Normalization is a technique used to normalize the inputs of a layer within a mini-batch. It helps in reducing internal covariate shifts, leading to accelerated convergence during training. By normalizing the inputs, batch normalization improves the stability and generalization of the network.

- Rectified Linear Unit (ReLU):

ReLU is an activation function that introduces nonlinearity to the model by outputting the input for positive values and zero for negative values (Equation 4). The ReLU layer maintains the size of the input, with the x and y dimensions being the same. Essentially, the ReLU functions as a truncation carried out individually for each element within the input. The primary objective of incorporating ReLU in a CNN is to enhance its nonlinearity. Given that the semantic information in images involves complex relationships, the CNN's input-to-output mapping must exhibit strong nonlinearity. Despite its simplicity, the ReLU function serves this purpose by introducing a nonlinear element, as depicted in Figure 1 [29].

$$ReLU = \begin{cases} 0, & \text{if } x < 0 \\ x & \text{if } x \geq 0 \end{cases} \quad [4]$$

- Dropout:

Dropout is a regularization technique used to prevent overfitting in neural networks. During training, random units in the network are “dropped out” by setting their weights to zero. This helps prevent the network from relying too much on specific neurons, thus promoting more robust and generalized learning.

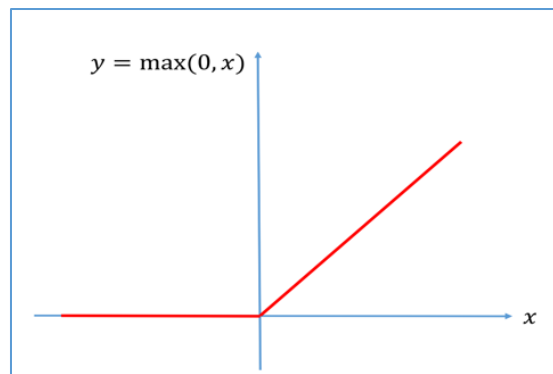


Fig. 1: ReLU function

- Global Average Pooling (GAP):

GAP is a technique used to reduce the spatial dimensions of the input while preserving important features. Unlike traditional fully connected layers, GAP calculates the average value of each feature map across its entire spatial dimensions. It reduces the number of parameters and helps prevent overfitting.

- Fully Connected (FC) Layer:

FC layers connect every neuron in one layer to every neuron in the next layer. These layers are often used towards the end of the CNN architecture to combine high-level features and make predictions. The FC layer comprises neurons that establish direct connections with neurons in the two neighboring layers, without establishing connections with any layers in between. This arrangement shows how neurons are organized in conventional types of ANNs [30].

- Softmax:

The softmax layer serves as an effective means for illustrating categorical distribution. It predominantly employs the softmax function in the output layer, which entails normalizing the exponentiated output values. This function, being differentiable, signifies a probability associated with each output. The exponential component contributes to enhancing the probability of the maximum value. The softmax equation can be expressed as follows:

$$o_i = \frac{e^{z_i}}{\sum_{i=1}^M e^{z_i}} \quad [5]$$

In softmax, the output for category i is then normalized to give o_i , the output features are z_i for category i, and the number of output nodes is M [31].

In sum, CNNs are breakthroughs in the science of computer vision that use the convolutional layers, batch normalization, ReLu activation, dropout, global average pooling, fully connected layers, and softmax activation methodologies to autonomously extract and learn hierarchical pattern features from the image data and precisely classify the objects and other visual objects regardless of the input dimensions and size.

4.2 Standard Autoencoder

One of the regular autoencoder's major steps is compressing the image into a smaller set of numbers. First, the entrance of the data is altered using encoding into code hidden. An activation function, such as the sigmoid or hyperbolic tangent, is used as a step function for the input data to enable transformation. The y-intercept (b) and slope (w) are the activations function's parameters that determine its curves. The coded data are the output that correlates to the size of the data used.

Second, the encoding phase is the same as decoding in disguise; it means that input data is formulated by decoding. Out of reconstruction processes, another set of weights and biases is involved that gives the result when applying the activation function (ϕ). The emitted output, if not otherwise stated, ought to closely mimic the given input data.

Further, the error squares between the original input data and the output reconstruction are calculated to evaluate the autoencoder performance. This error is called the quadratic error cost function; it can be done by the squared Euclidean distance. The autoencoder, especially suitable for image and audio processing, has been used in the fields of 3D mask synthesis, image denoising, and recognition. The reduction is achieved by these iterative processes [32].

4.3 CAE

CAE is the encoder in a built-in feature of the standard autoencoder being replaced by a convolutional layer. It has many convolutional layers in it, and the convolutional layers are powerful for structured grid-like data such as images. Similar to the simple autoencoder, the input layer and output layer have the same size. While CAE uses transposed convolutional layers for the decoder network, in the convolutional autoencoder the decoder network is used. Thus, the used architecture is made of convolutional layers in the encoder and transposed convolutional layers in the decoder, and they are responsible for feature extraction and decomposition. As shown in Figure 2, CAE represents data encoded and passing through a deep learning model. The encoder part includes convolutional layers for encoding the data input, and the decoder utilizes the transposed convolution layers to decipher the original input. Through adaptation, going to a more spatial hierarchy is possible than in a completely connected design. Each convolutional layer is characterized by a set of parameters, which mostly play the role of forming the receptive field and the output feature space on each layer. All these parameters directly influence the general performance and capacity of the convolutional machine autoencoder system.

The main idea of a CAE (a kind of neural network) is to determine a kind of compressed representation or code for each of the samples by minimizing the mean square error(s) between the input and the output. In CAE, two layers correspond to the encoder $fW(\cdot)$ and the decoder $gU(\cdot)$. These layers are modified to include convolutional operations. The encoder part $fW(\cdot)$ typically involves convolutional layers that capture spatial hierarchies and patterns in the input data. The decoder $gU(\cdot)$ consists of transposed convolutional layers to reconstruct the original input from the encoded representation. For a fully connected autoencoder, the encoder and decoder functions can be expressed as follows (Equations 6 and 7):

$$f_w(x) = \sigma(Wx) \equiv h, \quad [6]$$

$$g_u(h) = \sigma(Uh), \quad [7]$$

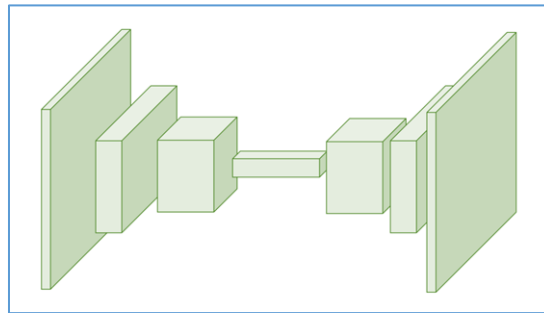


Fig. 2: Convolutional autoencoder structure

where x represents the input vector; h is the embedded code or representation; σ is an activation function (e.g., ReLU or sigmoid); and W and U are the weight matrices associated with the encoder and decoder, respectively. The bias terms are omitted for simplicity. During training, CAE minimizes the MSE between the input and output over all samples, following the objective function as follows:

$$\min_{w,u} \frac{1}{n} \sum_{i=1}^n \|g_u(f_w(x_i)) - (x_i)\|_2^2 \quad [8]$$

After training, the embedded code h serves as a new, more compact representation of the input sample, capturing essential features and patterns in the data. This compressed representation is often useful for various tasks such as image reconstruction, denoising, or feature extraction [33].

5. METHODOLOGY

The method involves feature extraction using a CAE curve, which is essentially a deep learning architecture long known to be relatively proficient in extracting compact and well-informative solutions of the provided data. In the light of ALL diagnoses, CAE can be similar to professionally recognizing main points from lymphoblast cell images, resulting in correct classification. A CAE that enables essential features that characterize lymphoblast ALL, such as size and texture, while still maintaining details of the original image during the extraction process was created to obtain informative features from lymphoblast cell images. The CAE architecture contains three convolutional parts for the encoder; each part has a convolutional layer, a leaky RELU activation layer, and a max pooling layer. This decision is, therefore, based on the hierarchical nature of the features of images, which play a vital role in CAE because as the network progresses, it goes through more abstract representations. Within each block of convolutional layers, the number of filters is less than three due to the dimensions of the images ($450 \times 450 \times 3$). A network with three filters per layer can be equipped with higher spatial resolutions because it can be employed to determine patterns and textures in lymphoblast cell images. The numbers of convolution kernels in the first last layers were set as 9, 27, and 27, respectively, enabling details extraction from images at multiple levels of abstraction. The initial layer with 9 kernels focuses on detecting basic features such as edges and textures. Progressing deeper into the network, the number of kernels was increased to 27 in the subsequent layers to capture more complex and abstract features. Leaky ReLU activation functions were involved to treat the problem of death neurons by permitting a gradual flow of small non-zero gradients in which the unit is inactive. Feature extraction must learn infrequent or negative examples. However, this robustness ensures it still discovers informative features providing high accuracy and a low error rate. The decoder was built with the opposite structure of the encoder with the depth-to-space layer applied instead of the pooling function to expand the depth of the image to the original image size for better image reconstruction. This selection is important because it enables a good portrayal of input images while simultaneously preserving the spatial cues, crucial for ALL cells to be captured as they are. The arrangement of the CAE's bottleneck layer is similar to the transforming feature maps from 2D to 1D, and its size is $67,500 \times 1$. This "squished" model is designed was represent significant aspects of input images for efficient feature extraction that could be helpful in the subsequent neural network classifier. States from the encoded one-dimensional feature space are very descriptive because they may be applied in mapping the lymphoblast cell images through the decoder. The reviving of the process (reconstructing) guarantees that less-important aspects, such as the cell size, shape, and texture, are well-

preserved, which, in turn, gives the extracted features credibility when considering them for leukemia diagnosis. In addition, hierarchical convolutions in CAE enable the detection of hierarchical features that are determined by either local or global neighbors of ALL cells. This system adoption advances the capability of the model to identify the minuscule differences between normal white blood cells and cancerous leukemic blasts, thus enhancing the diagnostic precision. Fig. 3 presents the structure of the CAE with which the learnable parameters and the convolution operator are associated. Around 15.9k of the learnable parameters are employed in the network, and they could be affected by the environment while the training stumbles on the feature extraction and reconstruction performance.

After features are automatically encoded using CAE, the extracted features are processed by CNN for final classification. Here, the developed CNN model decreases the time of ALL diagnosis and keeps it robust and accurate.

The CNN structure introduces discriminative features and categorizes lymphoblast cell images; however, this structure is carefully configured to classify them into leukemia and normal conditions. The CNN architecture part was built using two convolutional blocks made up of 1D convolutional layers, followed by batch normalization layers, ReLU activation layers, and layer normalization layers. This design plan aims at retaining important features of the high-dimensional space seen through CAE dynamics and encouraging stability and efficiency of the training algorithm. Within every convolutional layer, these 1D convolutional slots are employed to process the feature space moving across spatial patterns and structural element extractions. The feature space generated by the CAE was felled to 67,500 features for each sample. Thus, the size of the filter was chosen to be 32 to insert this and consider the vast nature of the feature space, further demonstrating that the larger filter size applied in CNN can efficiently capture intricate spatial interconnection and patterns across the lymphoblast cell images. In the first level of the convolutional layer, 40 filters were used to completely grab the significant information aspects of the data for leukemia detection. Meanwhile, 80 filters were deployed in the second convolution layer to move one step further but towards refining the feature representations and building more weak points against the pattern to be identified. The decision to use these 40 filters was based on optimizing CNN's ability to extract and refine features necessary for accurate classification of lymphoblast cell images. In the initial layer, 40 filters were employed to comprehensively capture significant information aspects from the data relevant to leukemia detection. This number strikes a balance between capturing diverse spatial patterns and maintaining computational efficiency. As the network progressed to the second convolutional layer, increasing the number of filters to 80 allowed for a deeper exploration of feature representations. This higher filter count enhanced the network's capability to discern finer details and subtle variations in the images, thereby refining the feature maps to better differentiate between leukemia and normal conditions. This hierarchical approach ensures that the CNN can effectively learn and represent complex patterns essential for precise classification, ultimately improving diagnostic accuracy in clinical applications. Thus, feature map design guarantees that the CNN could be able to properly discern the representation features for the input data in a wide scope. Hence, correct classification could be facilitated. Dropout with a rate of 0.5 was employed after each convolutional block to avoid overfitting the training set and to boost the generalization ability of the model. The dropout layer randomly zeroes out a fraction of input units during the training, so that the network is not highly dependent on interconnections between the neurons and does not over-rely on a few specific features or patterns in training data by avoiding that. The dropout rate of 0.5 (50%) is a commonly used heuristic in deep learning. It strikes a balance between reducing overfitting by regularizing the network and maintaining sufficient information flow during training. This rate has been found effective in preventing co-adaptation of neurons and promoting robust feature learning, contributing to better generalization of the model across different datasets and conditions. The CNN architecture comes to an end with a global average pooling layer whose task is to sum up all the spatial information from each feature map, and then a fully connected layer and softmax layer classify the image. The global average pooling layer creates a reduction in the spatial and dimensional aspects of the feature matrix. It keeps the important information while simplifying the classification process. Figure 4 shows the architecture of the designed CNN for the detection of ALL, its network structure, and the approximately 86.5 million learnable parameters' distribution. Network design complexity is an important feature when diagnosing leukemia clinically, and it asks for a developed solution to correctly classify lymphoblast cell images.

Layer name	Number of learnables
Input	0
Convolutional 2D	252
Leaky ReLU	0
Average pooling	0
Convolutional 2D	2214
Leaky ReLU	0
Average pooling	0
Convolutional 2D	6588
Leaky ReLU	0
Flatten	0
Depth to space	0
Convolutional 2D	6588
Leaky ReLU	0
Depth to space	0
Convolutional 2D	252
Leaky ReLU	0
Depth to space	0
Convolutional 2D	30
Leaky ReLU	0
Output	0

Fig. 3: Structure of the designed CAE and its learnable parameters

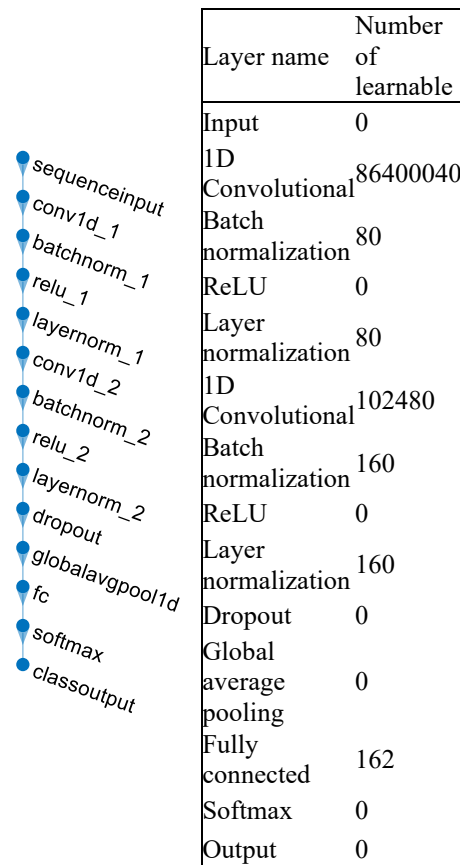


Fig. 4: Structure of the designed CNN and its learnable parameters

6. EVALUATION METRICS

Multiple reliability measurement tools, including accuracy, precision, recall, and F1 score, were used to assess the CNN model for diagnosing leukemia.

1. Accuracy:

Precision gives us an idea of the ratio of accurately predicted instances to the total instances, and accuracy provides us with the overall correctness of the model. Accuracy at a high level indicates precision with which ALL and HEM instances are labeled correctly.

$$Accuracy = \frac{TP+TN}{TP+TN+FP+FN} \quad [9]$$

2. Precision :

Accuracy means a probability that test data classify the nearest label what be a positive outcome of a model. Recall is determined by the number of true positives divided by the total true positives + false negatives. Accuracy was measured by determining the number of correctly made diagnoses among all the predicted cases that fit the diagnosis of ALL.

$$Precision = \frac{TP}{TP+FP} \quad [10]$$

3. Recall:

Recall, another more term for sensitivity, implies the capacity of the model to accurately identify all background instances of a specific class. The indicator is a proportion of the real all cases that are diagnosed and detected in a healthcare facility. It demonstrates that the model is capable of covering ALL cases, thus minimizing the possibility of false negative outcomes.

$$Recall = \frac{TP}{TP+FN} \quad [11]$$

4. F1 Score:

The F1 score is the averaging mean of precision and recall. It splits the positive and negative comments even if negative comments are not enough to be even. Therefore, this algorithm is beneficial when the ratio of positive and negative instances in the dataset is not balanced.

$$F_1Score = \frac{2 \times (Precision \times Recall)}{Precision + Recall} \quad [12]$$

The fever classification model observes that instances correctly classified as ALL are under true positives (TPs), whereas instances correctly classified as HEM are under true negatives (TNs). Meanwhile, instances incorrectly classified as ALL are under the FP category, and instances incorrectly classified as HEM come under the FN category.

7. SIMULATION RESULTS

A complete account of detailed studies carried out on the proposed method of ALL diagnosis was presented. MATLAB 2023b was used as the opening software for the planned technology.

7.1 Adjustments of CAE

The parameters were carefully set during CAE training to obtain the best feature extraction. Thus, the equilibrium of the process of convergence was squeezed between the speed convergence and stability by setting the learning rate to 0.001. Here, the parameter selection plus a large batch size of 6 proportionately utilize system resources and employ memory, thus providing efficient training cycles that smoothly operate.

The ADAM optimization algorithm was used for training the CAE because it can easily adjust for changing learning rates and it is more efficient when handling complex optimization areas. The recognition algorithms of ADAM can obtain informative representations of the input lymphoblast cell images through its potential capabilities. The process of how the training occurs is shown in Figure 5, where the number of epochs improved, and the construction of loss decreased progressively.

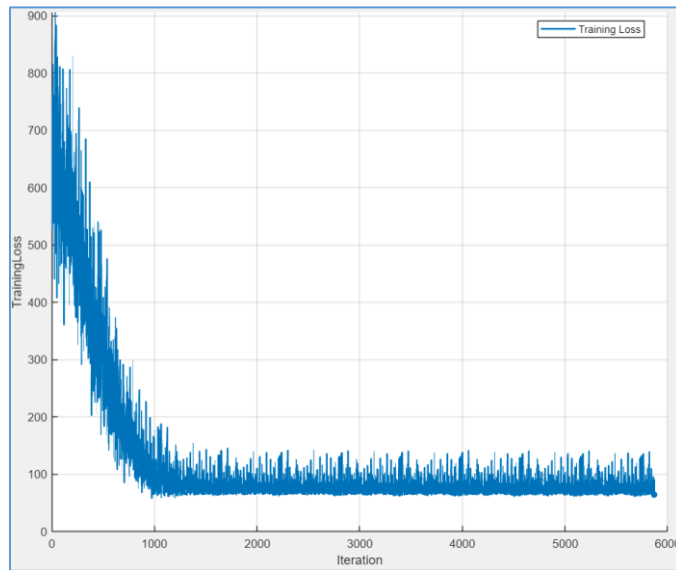


Fig. 5: Training progress of the designed CAE

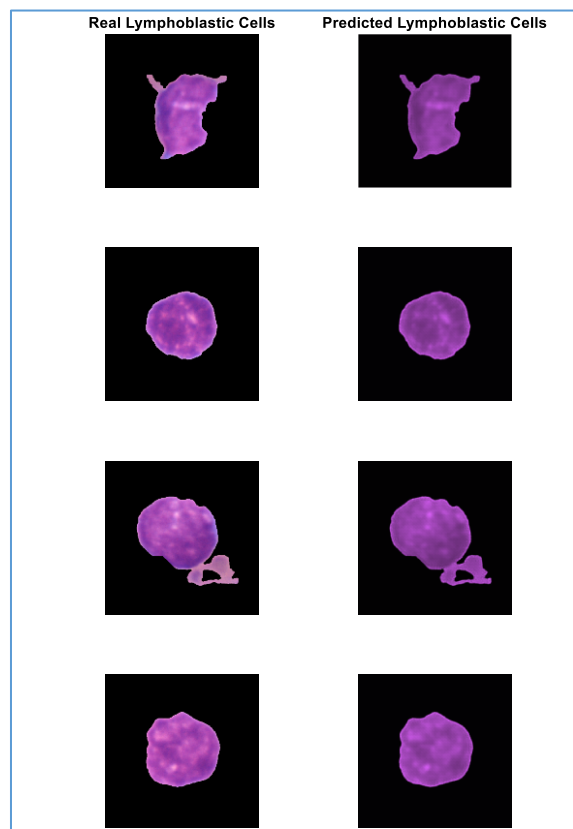


Fig. 6: Results of reconstruction of acute lymphoblastic leukemia cell images using the trained CAE

Post-training evaluation focuses on assessing the regenerative capability of the CAE and evaluating its proficiency in capturing salient features from the input images. Figure 6 presents the reconstructed images generated by the trained CAE, demonstrating its ability to reproduce key patterns and structures present in the original images.

The correlation coefficient between the reconstructed lymphoblastic cells and the original images was computed, as depicted in Figure 7, to further explore the reconstruction performance. The obtained correlation coefficient of 0.987 underscores the remarkable ability of CAE in capturing essential characteristics of the input images, thus highlighting its efficacy as a feature extraction tool for leukemia diagnosis.

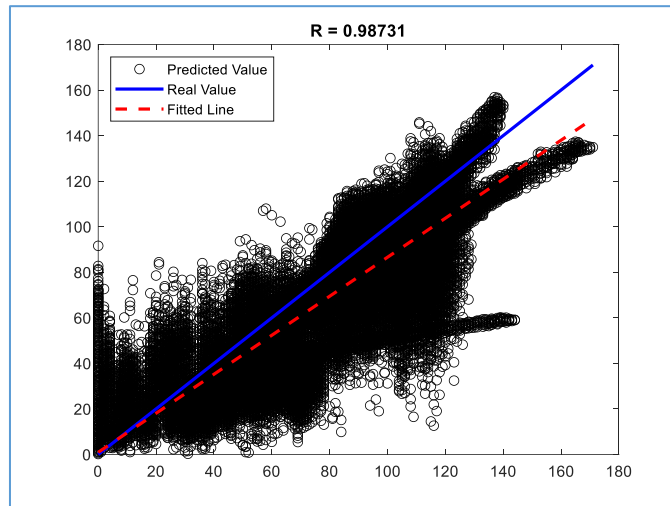


Fig. 7: Correlation coefficient of lymphoblastic leukemia cell image reconstruction

7.2 Adjustments of CNN Classifier

After the performance of CAE was evaluated, the CNN classifier was assessed. In this regard, optimizing various parameters is crucial for effective training of CNN. Selecting a maximum of 15 epochs ensures convergence without the risk of overfitting, balancing model complexity and training time. A learning rate of 0.001 was chosen for its stability in convergence and its ability to allow subtle adjustments to weights during optimization, adapting well to dataset intricacies.

The learning rate drop factor of 0.1 was used for training. It dynamically adjusts the learning rate, thus making a precise adjustment for parameters of the model, escaping from unfair local minima, and lowering the time required for optimizing. The CNN obtains a balance between the gradient parameter improvement and computational performance by having a batch size of 16, thus speeding up the training process.

Several assessments were conducted to measure the effectiveness of the setup, and various metrics were used, including accuracy, precision, recall, F1-score, receiver operating characteristic (ROC) curve, and confusion matrix analytics, providing a statistically significant insight into the model performance of classifying patients with leukemia from those without leukemia. The currently established techniques and the proposed approach were compared to show the latter's robustness and high efficiency in tackling leukemia diagnosis challenges.

7.3 Confusion Matrix

The learning rate drop factor of 0.1 was used for training. It dynamically adjusts the learning rate, thus making a precise adjustment for parameters of the model, escaping from unfair local minima, and lowering the time required for optimizing. The CNN obtains a balance between the gradient parameter improvement and computational performance by having a batch size of 16, thus speeding up the training process.

Thereafter, several assessments will be conducted to measure the effectiveness of the setup and a variety of metrics will be used. The model assessment will include accuracy, precision, recall, F1-score, ROC curve, and confusion matrix analytics providing a statistically significant insight into the model performance of classifying the leukemia patients from non-leukemia patients. Alongside that, a comparison between the currently established techniques demonstrating the proposed approach's robustness and high efficiency in tackling leukemia's diagnosis challenges will be carried out.



Fig. 8: Confusion matrix for training data



Fig. 9: Confusion matrix for test data

7.4 ROC

ROC curves have instrumental roles in the study of three separate operations: conducting the proposed diagnosis method, differentiating ALL and Hem classes, and optimizing the method. The ROC curves are shown in Figures 10 and 11, representing the types of discrimination connected to the test phase that constitute the visual demonstration of the model's discriminatory capabilities. A trade-off between sensitivity and specificity is effectively displayed to understand the model's performance along with the different thresholds. The highest range of performance is shown by the trend towards the top left-hand corner, which is a symptom of high sensitivity and low FP rates. The ROC curves exhibited value in assessing the precise diagnostic ability of the model. They can describe the model's ability to choose classes of leukemia with the best possible clinical medicine.

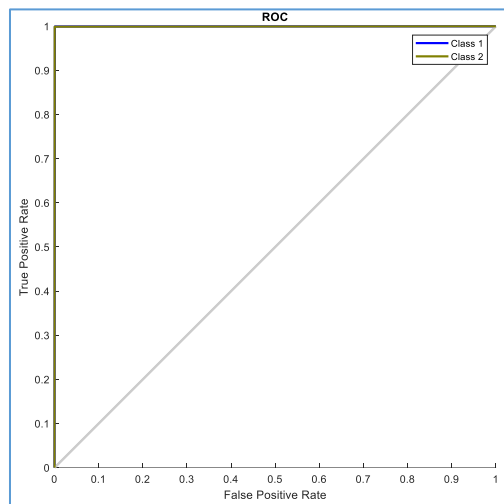


Fig. 10: ROC curve for training data

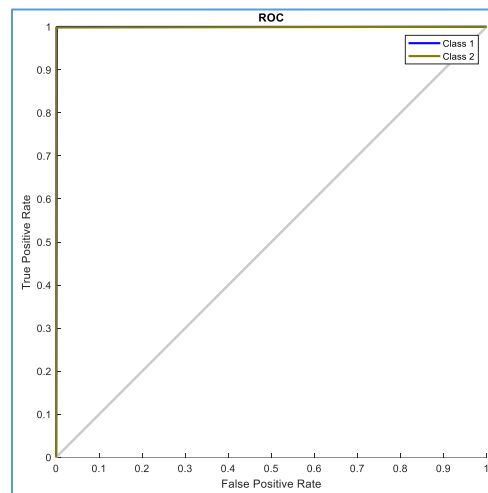


Fig. 11: ROC curve for test data.

7.5 Performance Investigation Using Evaluation Metrics

Figures 12 and 13 depict the results of leukemia diagnosis. These plot graphics demonstrate substantial advancement in terms of accuracy, which are 99.94% and 99.92% in the training and testing, respectively, with precision rates of 99.93% and 99.92%, respectively. Besides validating the outstanding potential of CAE in the process of feature extraction, the results further indicate the performance of the CNN algorithm. The network exhibited an extraordinary performance in classifying cells, demonstrated accurate diagnosis, and quickly and effectively showed the expected results.

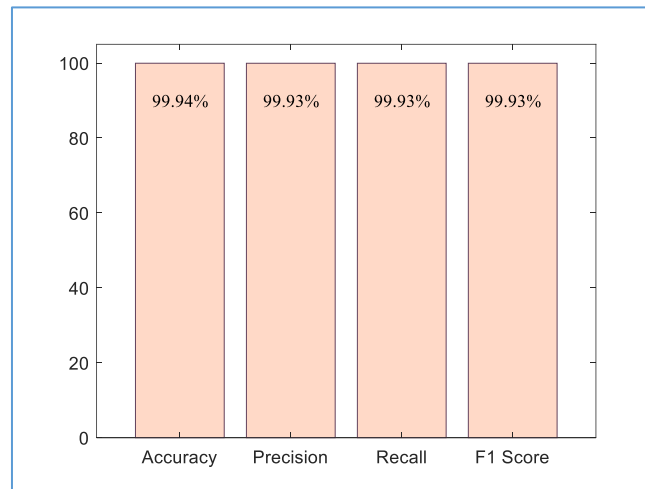


Fig. 12: Evaluation of the proposed method using evaluation metrics for the training dataset.



Fig. 13: Evaluation of the proposed method by using evaluation metrics for the test dataset.

8. COMPARISON

Paper [34] presents an ensemble strategy to automatically detect ALL cells in contrast to normal WBCs, structured in three stages: image preprocessing through oversampling to address unbalanced databases, deep spatial feature extraction using CNN alongside a gated recurrent unit (GRU) combined with bidirectional long short-term memory (BiLSTM) to capture long-distance dependencies and temporal features, and classification using a softmax function and a multiclass support vector machine (MSVM) classifier. This framework effectively classifies the C-NMC 2019 database into two categories, with a 90%–10% training-testing split, showcasing its novelty in the accurate diagnosis of ALL images. Despite utilizing existing tools, the proposed CNN-GRU-BiLSTM-MSVM framework demonstrates superior performance, with the DenseNet-201 model achieving an F1-score of 96.23% and an accuracy of 96.29% on the test dataset by using the MSVM classifier. These findings suggest that the proposed strategy can serve as a valuable complementary diagnostic tool for ALL and encourage further research to augment rare databases like blood microscopic images by integrating ML with deep learning algorithms for powerful diagnostic applications. A novel dataset of 500 peripheral blood smear images, featuring normal, AML, and ALL images, was introduced in [35]. The proposed work achieved 97% accuracy for binary classification tasks, employing fine-tuned fully connected layers and the last three convolutional layers of VGG16, as well as 98% accuracy for DenseNet121 along

with SVM. In the three-class classification task, an accuracy of 95% was attained for ResNet50 along with SVM.

Study [36] introduced a noninvasive diagnostic approach based on CNN using medical images. The proposed solution leverages a CNN model incorporating an Efficient Channel Attention (ECA) module with the Visual Geometry Group (VGG16) architecture from Oxford to enhance the extraction of deep features from the image dataset, resulting in improved feature representation and classification accuracy. The ECA module effectively addresses the morphological similarities between ALL cancer cells and healthy cells. Various data augmentation techniques were employed to enhance the quality and quantity of the training data. The study utilized the Classification of Normal vs. Malignant Cells (C-NMC) dataset, divided into seven folds to account for subject-level variability, a factor often overlooked in previous methods. The experimental results demonstrated that the proposed CNN model successfully extracted deep features, achieving an accuracy of 91.1%. These findings suggest that the proposed method can effectively diagnose ALL and assist pathologists in their diagnostic efforts.

However, the proposed method outperformed other previous methods, achieving an accuracy of 99.92%. Table 1 shows the comparison of the proposed method with other mentioned methods.

Table 1: Comparison of the proposed method with previous methods

Reference	Method	Accuracy	Dataset	Feature extraction
[34]	CNN-GRU-BiLSTM-MSVM	96.29%	C-NMC (Data set prepared by AIIMS)	Based on CNN
[35]	Fine-tuned VGG16 + SVM (Binary Classification)	97%	C-NMC (Data set prepared by AIIMS)	Based on CNN
	DenseNet121 + SVM (Binary Classification)	98%		
	ResNet50 + SVM (Three-class Classification)	95%		
[36]	Convolutional Neural Networks (CNNs)	91.1%	C-NMC (Data set prepared by AIIMS)	Based on CNN
Proposed method	Convolutional Autoencoder + CNN	99.92%	C-NMC (Data set prepared by AIIMS)	Based on CNN

9. CONCLUSION

This work significantly advances leukemia diagnosis by introducing a novel and effective deep learning-based approach. The main contribution lies in the integration of a CAE for feature extraction with a CNN or classification. The proposed approach demonstrates exceptional accuracy and precision, with the CAE

effectively capturing essential features of lymphoblast cell images and the CNN robustly classifying these features to distinguish between leukemia and healthy cells. By leveraging hierarchical convolutions and advanced optimization techniques, this method not only enhances diagnostic precision but also speeds up the diagnosis process, making it a valuable tool for early detection and timely intervention in clinical practice. The high correlation coefficient and performance metrics underscore the method's potential to revolutionize leukemia diagnostics through automated, reliable, and efficient deep learning technologies.

The CAE showed high accuracy in the feature extraction work, with a notable correlation coefficient of 0.987 for rebuilt images of lymphoblastic cells. This finding shows CAE's skills that are decisive in fetching the key points essential in the diagnosis of leukemia.

The latter shows the highest diagnostic accuracy, whereas CNN ranks second, with 99.92% precision in the diagnosis of ALL. The high accuracy remarkably proves the suitability and impressive recognition power of the CNN classifier in recognizing between leukemia and healthy cell images.

Feature extraction technique and classification using the CAE model constitute a favorable method to improve the classification rates and performance of leukemia classification. The implementation of the suggested method, which involves the use of deep learning technologies along with automating the diagnostic process, could introduce a revolutionary approach to the diagnosis of leukemia, leading to early detection and timely intervention.

However, this study has several limitations and challenges that warrant further investigation. The dataset size and diversity remain a concern because a larger and more varied dataset is crucial for ensuring the model's robustness and generalizability. Additionally, the substantial computational resources required for training the CAE and CNN models may limit their practical application in resource-constrained clinical settings. Potential overfitting, despite dropout layers, and the lack of interpretability of deep learning models pose challenges, necessitating more transparent and explainable AI techniques to gain clinical trust.

Future work should focus on acquiring larger and more diverse datasets, optimizing model architectures for efficiency, and integrating explainable AI methods to improve interpretability. Real-time implementation and extensive field testing in clinical settings could provide valuable feedback for further refinement. Exploring the integration of other diagnostic modalities and developing continuous learning systems could enhance the model's diagnostic accuracy and adaptability. Addressing these limitations and challenges could considerably advance the practical applicability and reliability of deep learning approaches in leukemia diagnosis, paving the way for early detection and timely intervention.

funding

"The authors declare that no funding was received for this research."

Acknowledgment

The authors would like to express their sincere gratitude to the **reviewers** for their valuable feedback, insightful comments, and constructive suggestions, which significantly contributed to enhancing the quality of this research. Their detailed evaluations and recommendations have been instrumental in refining the manuscript to meet the highest academic standards.

References

- [1]. Gupta, R., Gehlot, S., & Gupta, A. (2022). C-NMC: B-lineage acute lymphoblastic leukaemia: A blood cancer dataset. *Medical Engineering & Physics*, 103, 103793.
- [2]. Fathi, E., Rezaee, M. J., Tavakkoli-Moghaddam, R., Alizadeh, A., & Montazer, A. (2020). Design of an integrated model for diagnosis and classification of pediatric acute leukemia using machine learning. *Proceedings of the Institution of Mechanical Engineers, Part H: Journal of Engineering in Medicine*, 234(10), 1051-1069.
- [3]. Hauser, R. G., Esserman, D., Beste, L. A., Ong, S. Y., Colomb Jr, D. G., Bhargava, A., ... & Rose, M. G. (2021). A machine learning model to successfully predict future diagnosis of chronic myelogenous leukemia with retrospective electronic health records data. *American journal of clinical pathology*, 156(6), 1142-1148.



- [4]. Simsek, E., Badem, H., & Okumus, I. T. (2022). Leukemia Sub-Type Classification by Using Machine Learning Techniques on Gene Expression. In Proceedings of Sixth International Congress on Information and Communication Technology: ICICT 2021, London, Volume 4 (pp. 629-637). Springer Singapore.
- [5]. Warnat-Herresthal, S., Perrakis, K., Taschler, B., Becker, M., Baßler, K., Beyer, M., ... & Schultze, J. L. (2020). Scalable prediction of acute myeloid leukemia using high-dimensional machine learning and blood transcriptomics. *Iscience*, 23(1).
- [6]. Mahmood, N., Shahid, S., Bakhshi, T., Riaz, S., Ghufraan, H., & Yaqoob, M. (2020). Identification of significant risks in pediatric acute lymphoblastic leukemia (ALL) through machine learning (ML) approach. *Medical & Biological Engineering & Computing*, 58, 2631-2640.
- [7]. Dasariraju, S., Huo, M., & McCalla, S. (2020). Detection and classification of immature leukocytes for diagnosis of acute myeloid leukemia using random forest algorithm. *Bioengineering*, 7(4), 120.
- [8]. Abunadi, I., & Senan, E. M. (2022). Multi-method diagnosis of blood microscopic sample for early detection of acute lymphoblastic leukemia based on deep learning and hybrid techniques. *Sensors*, 22(4), 1629.
- [9]. Lee, J., Cho, S., Hong, S. E., Kang, D., Choi, H., Lee, J. M., ... & Kim, Y. (2021). Integrative analysis of gene expression data by RNA sequencing for differential diagnosis of acute leukemia: Potential application of machine learning. *Frontiers in Oncology*, 11, 717616.
- [10]. Haider, R. Z., Ujjan, I. U., Khan, N. A., Urrechaga, E., & Shamsi, T. S. (2022). Beyond the in-practice CBC: the research CBC parameters-driven machine learning predictive modeling for early differentiation among leukemias. *Diagnostics*, 12(1), 138.
- [11]. Arunachalam, S. (2020). Applications of Machine learning and Image processing techniques in the detection of leukemia. *International Journal of Scientific Research in Computer Science and Engineering*, 8(2).
- [12]. Angelakis, A., & Soulioti, I. (2021). Diagnosis of acute myeloid leukaemia using machine learning. arXiv preprint arXiv:2108.07396.
- [13]. Sridhar, K., Yeruva, A. R., Renjith, P. N., Dixit, A., Jamshed, A., & Rastogi, R. (2022). Enhanced Machine learning algorithms Lightweight Ensemble Classification of Normal versus Leukemic Cel. *Journal of Pharmaceutical Negative Results*, 496-505.
- [14]. Monaghan, S. A., Li, J. L., Liu, Y. C., Ko, M. Y., Boyiadzis, M., Chang, T. Y., ... & Ko, B. S. (2022). A machine learning approach to the classification of acute leukemias and distinction from nonneoplastic cytopenias using flow cytometry data. *American journal of clinical pathology*, 157(4), 546-553.
- [15]. Karim, A., Azhari, A., Shahroz, M., Belhaouri, S. B., & Mustofa, K. (2021). LDSVM: Leukemia cancer classification using machine learning. *Comput. Mater. Contin*, 71(2), 3887-3903.
- [16]. Kashef, A., Khatibi, T., & Mehrvar, A. (2020). Treatment outcome classification of pediatric Acute Lymphoblastic Leukemia patients with clinical and medical data using machine learning: A case study at MAHAK hospital. *Informatics in Medicine Unlocked*, 20, 100399.
- [17]. Iswarya, M. (2022, May). Detection of Leukemia using Machine Learning. In 2022 International Conference on Applied Artificial Intelligence and Computing (ICAIC) (pp. 466-470). IEEE.
- [18]. Gupta, K., Jiwani, N., & Whig, P. (2022, September). Effectiveness of machine learning in detecting early-stage leukemia. In International Conference on Innovative Computing and Communications: Proceedings of ICICC 2022, Volume 2 (pp. 461-472). Singapore: Springer Nature Singapore.
- [19]. Sarder, M. A., Maniruzzaman, M., & Ahammed, B. (2020). Feature selection and classification of leukemia cancer using machine learning techniques. *Machine Learning Research*, 5(2), 18.



- [20]. Loey, M., Naman, M., & Zayed, H. (2020). Deep transfer learning in diagnosing leukemia in blood cells. *Computers*, 9(2), 29.
- [21]. Kang, A. S., Kang, L. C., Mastorides, S. M., Foulis, P. R., DeLand, L. A., Seifert, R. P., & Borkowski, A. A. (2021). Machine Learning Approaches to Automated Flow Cytometry Diagnosis of Chronic Lymphocytic Leukemia. arXiv preprint arXiv:2107.09728.
- [22]. Bibi, N., Sikandar, M., Ud Din, I., Almogren, A., & Ali, S. (2020). IoMT-based automated detection and classification of leukemia using deep learning. *Journal of healthcare engineering*, 2020, 1-12.
- [23]. Thanmayi A, V. L., Reddy, S. D., & Kochuvila, S. (2021). Detection of leukemia using k-means clustering and machine learning. In *Ubiquitous Communications and Network Computing: 4th EAI International Conference, UBIUNET 2021, Virtual Event, March 2021, Proceedings* (pp. 198-209). Springer International Publishing.
- [24]. Surya Sashank, G. V., Jain, C., & Venkateswaran, N. (2021). Detection of acute lymphoblastic leukemia by utilizing deep learning methods. In *Machine Vision and Augmented Intelligence—Theory and Applications: Select Proceedings of MAI 2021* (pp. 453-467). Springer Singapore.
- [25]. Bukhari, M., Yasmin, S., Sammad, S., El-Latif, A., & Ahmed, A. (2022). A deep learning framework for leukemia cancer detection in microscopic blood samples using squeeze and excitation learning. *Mathematical Problems in Engineering*, 2022.
- [26]. Gupta, R., Gehlot, S., & Gupta, A. (2022). C-NMC: B-lineage acute lymphoblastic leukaemia: A blood cancer dataset. *Medical Engineering & Physics*, 103, 103793.
- [27]. Li, Z., Liu, F., Yang, W., Peng, S., & Zhou, J. (2021). A survey of convolutional neural networks: analysis, applications, and prospects. *IEEE transactions on neural networks and learning systems*.
- [28]. Chauhan, R., Ghanshala, K. K., & Joshi, R. C. (2018, December). Convolutional neural network (CNN) for image detection and recognition. In *2018 first international conference on secure cyber computing and communication (ICSCCC)* (pp. 278-282). IEEE.
- [29]. Wu, J. (2017). Introduction to convolutional neural networks. National Key Lab for Novel Software Technology. Nanjing University. China, 5(23), 495.
- [30]. O'Shea, K., & Nash, R. (2015). An introduction to convolutional neural networks. arXiv preprint arXiv:1511.08458.
- [31]. Albawi, S., Bayat, O., Al-Azawi, S., & Ucan, O. N. (2017). Social touch gesture recognition using convolutional neural network. *Computational Intelligence and Neuroscience*, 2018.
- [32]. Chen, M., Shi, X., Zhang, Y., Wu, D., & Guizani, M. (2017). Deep feature learning for medical image analysis with convolutional autoencoder neural network. *IEEE Transactions on Big Data*, 7(4), 750-758.
- [33]. Zhang, Y. (2018, March). A better autoencoder for image: Convolutional autoencoder. In *ICONIP17-DCEC*. Available online: http://users.cecs.anu.edu.au/Tom.Gedeon/conf/ABCs2018/paper/ABCs2018_paper_58.pdf (accessed on 23 March 2017).
- [34]. Guo, X., Liu, X., Zhu, E., & Yin, J. (2017). Deep clustering with convolutional autoencoders. In *Neural Information Processing: 24th International Conference, ICONIP 2017, Guangzhou, China, November 14-18, 2017, Proceedings, Part II 24* (pp. 373-382). Springer International Publishing.
- [35]. Mohammed, K. K., Hassanien, A. E., & Afify, H. M. (2023). Refinement of ensemble strategy for acute lymphoblastic leukemia microscopic images using hybrid CNN-GRU-BiLSTM and MSVM classifier. *Neural Computing and Applications*, 35(23), 17415-17427.



- [36]. Abhishek, A., Jha, R. K., Sinha, R., & Jha, K. (2022). Automated classification of acute leukemia on a heterogeneous dataset using machine learning and deep learning techniques. *Biomedical Signal Processing and Control*, 72, 103341.
- [37]. Zakir Ullah, M., Zheng, Y., Song, J., Aslam, S., Xu, C., Kiazolu, G. D., & Wang, L. (2021). An attention-based convolutional neural network for acute lymphoblastic leukemia classification. *Applied Sciences*, 11(22), 10662.